GEOCHEMISTRY OF MAGMAS ERUPTED ALONG THE NORTHERN EAST PACIFIC RISE AT 6°-12° IMPLICATIONS FOR MANTLE SOURCE REGIONS AND INTRACRUSTAL EVOLUTIONARY PROCESSES

Research Thesis

Presented in Partial Fulfillment of the Requirements for graduation

with Research Distinction in Earth Sciences in the undergraduate colleges of

The Ohio State University

By

Lienne R. Sethna

The Ohio State University

May 2016

Approved by

Michael Barton, Advisor
School of Earth Sciences

TABLE OF CONTENTS

ABSTRACT

The East Pacific Rise (EPR) is a fast-spreading mid-ocean ridge characterized by several discontinuities including large transform faults and overlapping spreading centers. Current models for mid-ocean ridges correlate spreading rate with depth of partial crystallization of magmas; faster spreading ridges are coupled with shallower magma chambers. Anomalously high pressures and hence depths of partial crystallization have been calculated for some magmas erupted along the Northern EPR. One possible explanation is that ridge discontinuities are associated with cooler mantle and crust, promoting thermal arrest and crystallization of magmas at high pressures. An alternative view is that high rates of magma input into crustal reservoirs promotes melting and assimilation of crustal lithologies. Assimilation of crust can lead to anomalous compositions and calculated pressures for such compositions do not represent the actual pressure of magma evolution.

Geochemical analyses of lavas erupted along the EPR between ~6 and 12°N were compiled from Gale et al. (2013) and examined to identify evidence for assimilation of oceanic crust. This ridge segment was chosen because some samples yield anomalously high calculated pressures and hence depths of partial crystallization. The analyses were normalized to the composition of average Normal Mid-Ocean Ridge basalt (NMORB) to aid interpretation. Lavas erupted along the southern part of the ridge segment are depleted in highly incompatible elements, and are interpreted to have formed by melting of a depleted mantle source followed by crystallization en-route to the surface. Lavas erupted along the northern part of the ridge are not depleted in highly incompatible elements and formed by melting of a "normal" mantle source. However, some of these lavas have geochemical characteristics (enrichment in incompatible elements, high SiO_2) consistent with assimilation of crustal lithologies. Work in progress will determine whether there

is a correlation between these geochemical characteristics and high calculated pressures of partial crystallization.

ACKNOWLEDGEMENTS

I would first like to thank my family—Dad, Mom, Kim, brothers, and grandparents—for their constant support, encouragement, and confidence in me. Without them, I would have no passion for rocks, appreciation for hard work, nor funding for my education. Thank you to my dad for the endless hard questions to make me think, the laughs, and the French toast. You'll always be number one. Thank you to my mom for supporting my choices and believing in me. Thank you to my dear brothers—Cyrus, Darayus, and Devin. And thank you to my mom, Kim, for instilling in me the principles of feminism, and always being an example of how women can really have it all.

I would also like to thank my research advisor, Dr. Michael Barton for his guidance and support throughout this research project. I am also very grateful to Christina Zerda and Jameson Scott for their knowledge and suggestions. Also, a thank you to Yoko Miyakawa and Katherine Fleeman for being very helpful and very fun research mates.

A final huge thank you to my Ohio State professors, peers, and friends who made my college experiences memorable and worthwhile. Thank you School of Earth Sciences for making a big place seem small and investing time into making me grow individually as a scientist. Thank you to my best geofriend, Abbie Bowman, for conquering the journey to becoming a female geoscientist with me. And thank you to my best friend from the first day of college, Tony Davis, for always supporting my ambitions and being there for all the important moments.

You all rock.

LIST OF FIGURES

LIST OF TABLES

INTRODUCTION

The mid-ocean ridge system is a seventy-five thousand kilometer volcanic mountain chain and is by far one of the longest structures on Earth. It extends from the Arctic Ocean, around Asia, Australia, and Africa, and up the west coast of the Americas. Mid-ocean ridges are a boundary between two of Earth's tectonic plates, where molten rock rises to the surface from the mantle to generate new oceanic crust and lithosphere. This thesis will focus on a section of the East Pacific Rise (EPR) from ~6°N–12°N.

The EPR is considered a fast spreading ridge with spreading rates in the study region averaging ~104mm/year (Gale et al., 2013). Fast-spreading ridges are associated with higher heat and magma fluxes than are slow-spreading ridges. In warm, fast-spreading crust, magmas should ascend to shallow depths before they encounter cool, crustal rocks where heat loss promotes crystallization to form shallow reservoirs (Morgan & Chen 1993; Rubin & Sinton, 2007).

There is widespread agreement that the thermal structure of the crust at the axis of mid-ocean ridges is related to both the spreading rate and heat flux. The heat flux is largely controlled by the magma flux out of the mantle and this is a function of the depth at which the decompressing mantle intersects the solidus on the way to the surface. Several features of ridges, such as the gross morphology, cross-sectional profile, degree of segmentation (especially the density of transform offsets), volume of erupted magma (and hence magma flux), heat flow, and composition of erupted basalts are related to spreading rate (Macdonald, 2001).

The accretion of oceanic crust results from the crystallization of basaltic magma and there are three different models that describe this process at mid-ocean ridges. In one of these models (the Gabbro-Glacier model), magma crystallizes in a sill-like lens of melt that is typically only a few tens of meters thick (Sinton & Detrick, 1992; Rubin et al., 2009). The key feature of this model

is that crustal accretion occurs by crystallization in a very narrow depth interval (Figure 1a). In another model (the Crystal Mush model), a thin, shallow melt lens is underlain by a crystal "mush" extending down to the base of the crust (Figure 1b). In this model, crustal accretion occurs over a range of depths (Sinton & Detrick, 1993; Maclennan, 2004). In the third model (the Many Sill or Sheeted-Sill model), a shallow sill-like magma lens is underlain by crust containing multiple sills extending down to the base of the crust (Figure 1c). Crustal accretion occurs by crystallization sills sited throughout the crustal section, and will therefore also occur over a range of depths (Kelemen, 1997).

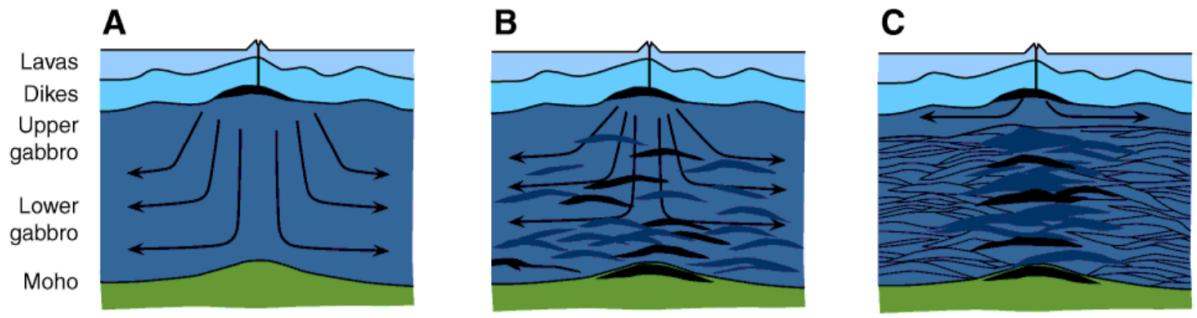

Figure 1. Models of crustal accretion. A) Gabbro-Glacier model with simple, ductile flow. B) Crystal Mush model with hybrid ductile flow and sill intrusions within a basal sill. C) Many Sill model (from Korenaga & Keleman, 1998)

Regardless of the exact accretionary model, mature oceanic crust shows remarkably little variation in seismic velocity structure over a wide range of spreading rates (Keller, 1992; Henstock et al., 1993). In addition, Keller (1992) and Bown & White (1994) showed that there is no significant variation in crustal thickness (or velocity structure) determined from well-constrained seismic refraction profiles for crust formed at half-spreading rates ranging from 15 to 75 mm/year These results show that the processes involved in crustal accretion are the same across a wide range of spreading rates. (Henstock et al., 1993).

While these models describe crustal accretion, they envisage different magma plumbing systems beneath ridge axes. With petrologic methods based on the compositions of basaltic melts, the depths of partial crystallization can be determined and can be used to establish the locations of magma bodies in the crust to reconstruct magma plumbing systems (Michael & Cornell, 1998; Herzberg, 2004; Almeev et al., 2008; Kelley & Barton, 2008). A combination of constraints on the depths of partial crystallization of basaltic melts obtained from petrological studies with those obtained from seismic studies should provide an accurate and internally consistent model for magma plumbing systems at mid-ocean ridges.

Dmitriev (1998), Michael & Cornell (1998) and Herzberg (2004) concluded that mid-ocean ridge basalts (MORB) can partially crystallize at pressures appropriate for the mantle (i.e. at sub-crustal depths). They also concluded that high pressure crystallization is common for MORB erupted along slow-spreading ridges, but not for those erupted along fast-spreading ridges. A study by Zerda (2014) yielded calculated pressures of partial crystallization that ranged up to 1000 MPa for the fast-spreading Northern EPR between 8°N and 15°N (Figure A15). These pressures are much higher than the pressures of partial crystallization (200-300 MPa) calculated for other ridge segments. The results for the East Pacific Rise are puzzling because the relatively high spreading rate and high magma flux (Rubin & Sinton, 2007) indicate that the underlying mantle is relatively warm and, as previously noted, magmas should be able to ascend to shallow depths in warm, fast-spreading crust before heat loss promotes crystallization, arrest of ascent, and formation of shallow reservoirs. The paradox of anomalously high pressures of partial crystallization calculated for samples from the fast-spreading EPR provides the rationale for the study described in this thesis.

Kelley & Barton (2008) and Lissenberg & Dick (2008) have proposed that processes such as assimilation to modify the compositions of basaltic melts and that pressures of partial crystallization calculated for these modified melt compositions do not represent the *actual* pressures of partial crystallization. These workers showed that calculated pressures can be anomalously high or anomalously low, depending on the exact nature of the assimilation process, relative to the actual pressures of partial crystallization.

To investigate the possibility that processes other than crystallization are involved in magma evolution along this segment of the EPR, this study uses the tools of trace element geochemistry to identify samples with compositions consistent with magma evolution via crust-mantle interaction. By looking at trace element compositions in the samples from ~6°N-12°N, we hope to provide the basis for explaining the anomalously high calculated pressures for some samples as the interaction of magma with oceanic crust, so that these pressures are not representative of the actual crystallization regime along the ridge.

Geologic Setting

Location

The East Pacific Rise (EPR) is part of a massive ocean feature known as a mid-ocean ridge, a boundary between two of Earth's tectonic plates and a place where molten rock rises to the surface from great depths. The area of study is a 750km section of the EPR, extending from about 6° to 12° N latitude, located 1100km off the west coast of Central America.

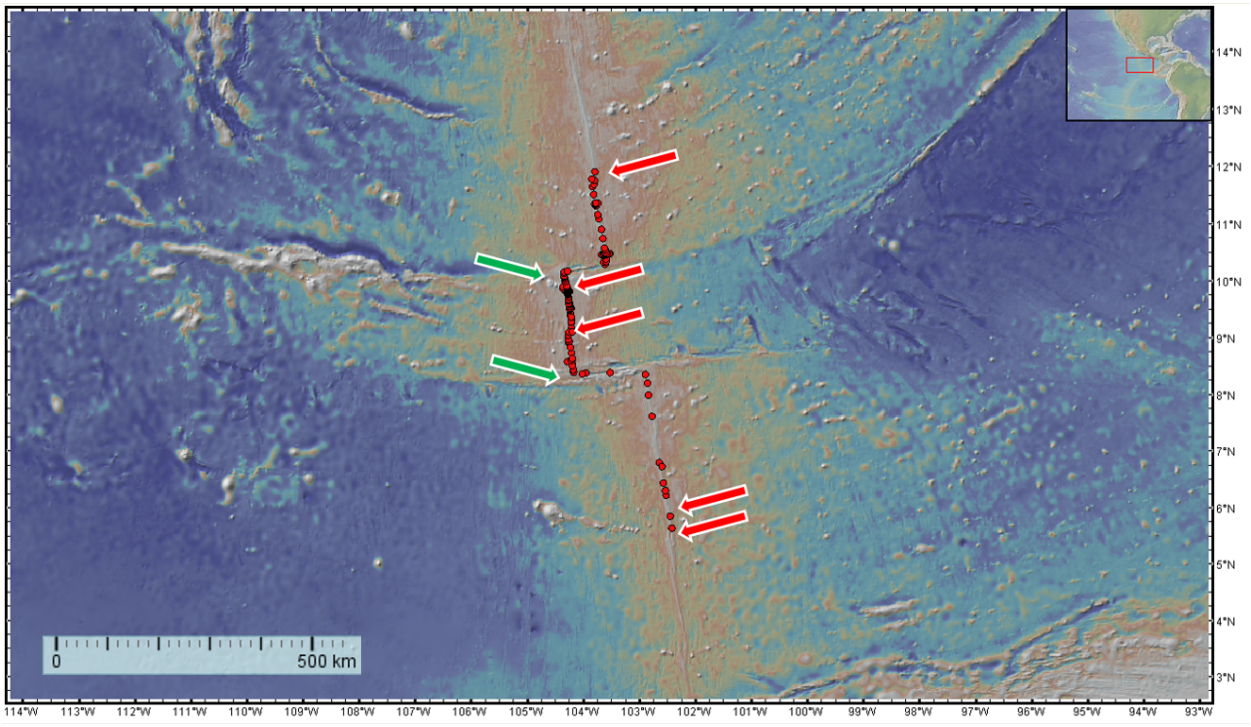

Figure 2. Location of samples (red dots), overlapping spreading centers (red arrows), and transform faults (green arrows). Created using GeoMapApp.

Topography

The topography of the EPR has been studied through a series of ocean mapping projects that used sonar technology to glean information about the sea floor. The axis of the ridge is elevated above the rest of the sea floor and segments of the ridge are offset by transform faults as the ridge adjusts for the curve of the Earth. An ocean mapping expedition by the Scripps Institution of Oceanography in San Diego, California found new features such as segments of the ridge that

were non-linear, overlapping ridges, and oceanic crust that was deformed and distorted around these features (Macdonald & Fox, 1990).

The EPR is considered a "fast" spreading mid-ocean ridge, spreading at full rates from 60 to 170 mm/year (Macdonald & Fox, 1990). This area of study has an average full spreading rate of 104 mm/year with increasing spreading rates going south along the ridge (94mm/year at the northernmost end to 114mm/year and the southernmost – Gale et al., 2013). Different ridges around the world have different spreading rates. For example, the Mid-Atlantic Ridge is a "slow" spreading mid-ocean ridge, spreading at an average full rate of 20–30 mm/year. The rate of spreading corresponds to the rate at which magma is supplied to the ridges and overflows onto the ocean floor. Therefore, the spreading rates also correspond with the topography of the crest of the ridges. A fast spreading ridge with a high rate of magma replenishment and uprising will have an elevated crest up to several hundred meters high and tens of kilometers wide, whereas slow-spreading ridges are characterized by deep, axial rift valleys (Macdonald & Fox, 1990).

The crest of the EPR separates the Pacific and Cocos tectonic plates; however, the crest is not a continuous feature along the EPR. As stated above, transform faults can offset the ridge by up to several hundred kilometers. At the transform faults, the tectonic plates move perpendicular to the length of the ridge, shearing against each other. There are two transforms included in this area of study – the Siqueiros at 8.37°N and the Clipperton at 10.67°N. Plate segments between two transform faults can sometimes move parallel to the length of the ridge – called a propagating rift (Macdonald & Fox, 1990).

Volcanology

The Woods Hole Oceanographic Institution developed a magma-supply model to find connections between segmentation of the ridge and volcanic activity (Macdonald & Fox, 1990).

Within the Earth, at depths between thirty to sixty kilometers, rocks are heated to extremely high temperatures but remain solid because of the extreme pressure experienced at those depths. However, where tectonic plates are spreading, there is an alleviation of pressure, and the rocks melt due to decompression melting. Since the now molten rock is less dense than solid rock, it ascends to fill the magma chamber below the oceanic crust that makes up the ridge (Francheteau, 1983). The ridge is then pushed up by the buoyant forces in the magma chamber, which is why ridges with high replenishment rates (and therefore faster spreading rates) have higher topography than slower spreading ridges. The rate and volume of the magma supply can vary between regions in the same ridge, meaning the morphology – shape – of the ridge can vary between regions.

METHODS

Data for the EPR from ~6-12°N were collected from a global database published by Gale et al. (2013). Over thirty-thousand individual samples were compiled, examined, and filtered to exclude any incomplete analyses or those judged to be of inferior quality. Each sample in the database has latitude and longitude, depth, and spreading rate information along with major oxide and trace element concentrations. From this global database, the analyses and interpretations made in this thesis come from just 251 of those samples recovered from latitude 5.642°N-11.913°N.

Microsoft Excel and CoHort Software were used to analyze and interpret these data. Excel was used to organize the data and calculate normalization values and spreading rates. Normalization calculations are described below. Spreading rates were taken from the Gale et al. (2103) and compared with the Lamont-Doherty Earth Observatory (LDEO) Ridge Spreading Rate Calculator (http://www.ldeo.columbia.edu/users/menke/plates.html). The spreading rates reported by Gale et al. were calculated using the NUVEL-1A model. This model is determined from average plate motions over wide time spans. This includes earthquake slip directions that report plate movement on the decade-century time scale, transform fault azimuths that report plate movement over hundreds of thousands of years, and mid-ocean ridge spreading rates that uniformly average plate motion over 3.16 Ma (DeMets et al., 2009). The LDEO Ridge Spreading Rate Calculator uses the NUVEL-1 Plate Velocity Parameters to calculate spreading rates given a latitude and longitude (DeMets et al., 1989).

The 251 samples were divided into ten different segments based on latitude as defined by Gale et al. (2013). Samples grouped into segments allows for more in depth analysis of the variations in concentrations and compositions along the ridge. Comparison of various compositions between

ridge segments allows processes such as crystallization, crustal assimilation, magma mixing, etc. to be inferred. The ten segments with their corresponding latitude are listed in Table A1.

To investigate the possibility that processes other than crystallization are involved in magma evolution, trace element geochemistry is used to identify samples with compositions consistent with magma evolution via crust-mantle interaction. CoHort Software was used to plot variations in major oxide and trace element compositions compared with other oxides, elements, or latitude. Trace elements constitute only a small portion of the mass of any system but they provide geochemical and geological information out of proportion to their abundance. This is possible because (1) there are far more trace elements than major oxides in essentially all natural samples, (2) the range of concentrations of many trace elements is much larger than the range in concentrations for major oxides, (3) trace elements show a strong preference for either the solid or the melt and are more sensitive to processes than major oxides would be, and (4) the behavior of trace elements is generally simpler than that of the major oxides, allowing simple, numerical methods to model the behavior of trace elements in natural processes (White, 1997).

Because each trace element has its own chemical properties, variations in its concentration can potentially provide information about the processes occurring in nature. Additionally, variations in the concentration of trace elements are useful for monitoring changes in the composition of magmas during melting and crystallization.

Variation diagrams of trace elements and oxides were plotted against magnesium oxide (MgO) to compare the composition of the magmas with that of the theoretical, predicted compositions that result from crystallization. Since MgO is removed from the melt by the crystallization of olivine, the MgO contents of magmas produced by crystallization should decrease in a steady and predictable way. Comparison of the relationship of trace element and oxide concentrations

with MgO concentrations of the samples allows determination of whether the magma compositions are related by crystallization alone or if other processes must have occurred during magma evolution (White, 1997).

Trace elements plotted against other trace elements are another method of determining processes affecting the composition of the magma. Because concentrations of incompatible elements should, theoretically, increase in residual melts at the same rate, linear relationships should be observed on plots of incompatible trace elements versus other incompatible trace elements.

In order to use trace element abundances to identify samples with anomalous compositions, it is useful first to establish the variations in abundances in magmas erupted along ridge segments. This is most easily accomplished using normalization plots (spidergrams) that show the concentrations of trace elements normalized to the concentrations in a reference rock or reservoir. Trace element concentrations were normalized to the values for average "Normal Mid-Ocean Ridge Basalt" (NMORB) composition and primitive mantle composition, whereas rare-earth element concentrations were normalized to values for a carbonaceous (CI) chondrite. The average NMORB composition is that given by Gale et al., (2013, Table A2), the primitive mantle compositions is given by Sun and McDonough, (1989, Table A3), whereas rare-earth element (REE) compositions for the CI chondrite are given by McDonough and Sun (1995, Table A4). Normalization was done by dividing the raw concentration for each element by the concentrations in each of the three "reference" compositions. This approach allows for rapid visual identification of samples that deviate from the composition of the reference compositions.

Finally, I compared MgO, SiO_2, K_2O/P_2O_5, and K/U versus latitude to constrain the possibility that crustal assimilation has occurred. The K_2O/P_2O_5 ratio was calculated using the Gale et al. (2013) values by dividing the concentration of K_2O by P_2O_5. The K/U ratio was also calculated

from Gale et al. (2013) values by converting K_2O into K weight percent ($\frac{K_2O \text{ concentration} \cdot 2 \cdot 39.0983}{94.196}$) and then dividing by the U concentration. Multiplication by 39.0983 for the atomic mass of K and by 2 for the number of K atoms, division by 94.196 for the total atomic mass of K_2O.

RESULTS

Spreading Rates

The average spreading rate for the East Pacific Rise from 5.642°N to 11.787°N from the NUVEL-1A model and reported by Gale et al. is 103.71 mm/year.

These rates vary from those calculated by the Lamont-Doherty Earth Observatory (LDEO), which uses NUVEL-1 Plate Velocity Parameters to calculate spreading rates. The NUVEL-1 model consists of earthquake slip vectors, transform fault azimuths, and spreading rates over a uniform interval of 3.0 Ma (DeMets et al., 1989). The average spreading rate for the East Pacific Rise from 5.642°N to 11.787°N using the NUVEL-1 model and calculated by LDEO is 108.82 mm/year (http://www.ldeo.columbia.edu/users/menke/plates.html).

I prefer the spreading rates calculated by Gale et al. because the NUVEL-1A model is more recent and are related to the data used in the following geochemical analyses. Although the spreading rates vary (<5%), it is conclusive that the EPR is a fast spreading ridge which affects the morphology, cross-sectional profile, degree of segmentation (such as the density of transform fault offsets), volume of erupted magma, heat flow, and the composition of the erupted basalts. The composition of the basalts erupted from this section of the EPR are discussed below.

Geochemical Analyses: Trace element plots versus MgO

The elements europium (Eu), ytterbium (Yb), samarium (Sm), copper (Cu), barium (Ba), strontium (Sr), and cesium (Cs) were plotted against magnesium oxide (MgO) to compare the variations of these elements in the basalt samples with the behavior expected for crystallization. MgO is compatible in olivine and its concentration in the melt decreases during cooling and crystallization (Reynolds, 1992). With the exception of a few outliers, most elements define arrays indicating incompatible behavior (concentrations increase as the MgO concentration

decreases and olivine is crystallized from the magma). The concentrations of Eu, Yb, and Sm all increase linearly as the MgO concentration in the melt decreases (Figure 3). The concentration of Cu decreases slightly as MgO decreases, Ba concentration increases slightly as MgO decreases, Cs concentration shows a wide range of values for MgO between 5-9 wt%, and Sr concentration remains relatively constant as MgO decreases (Figure 4).

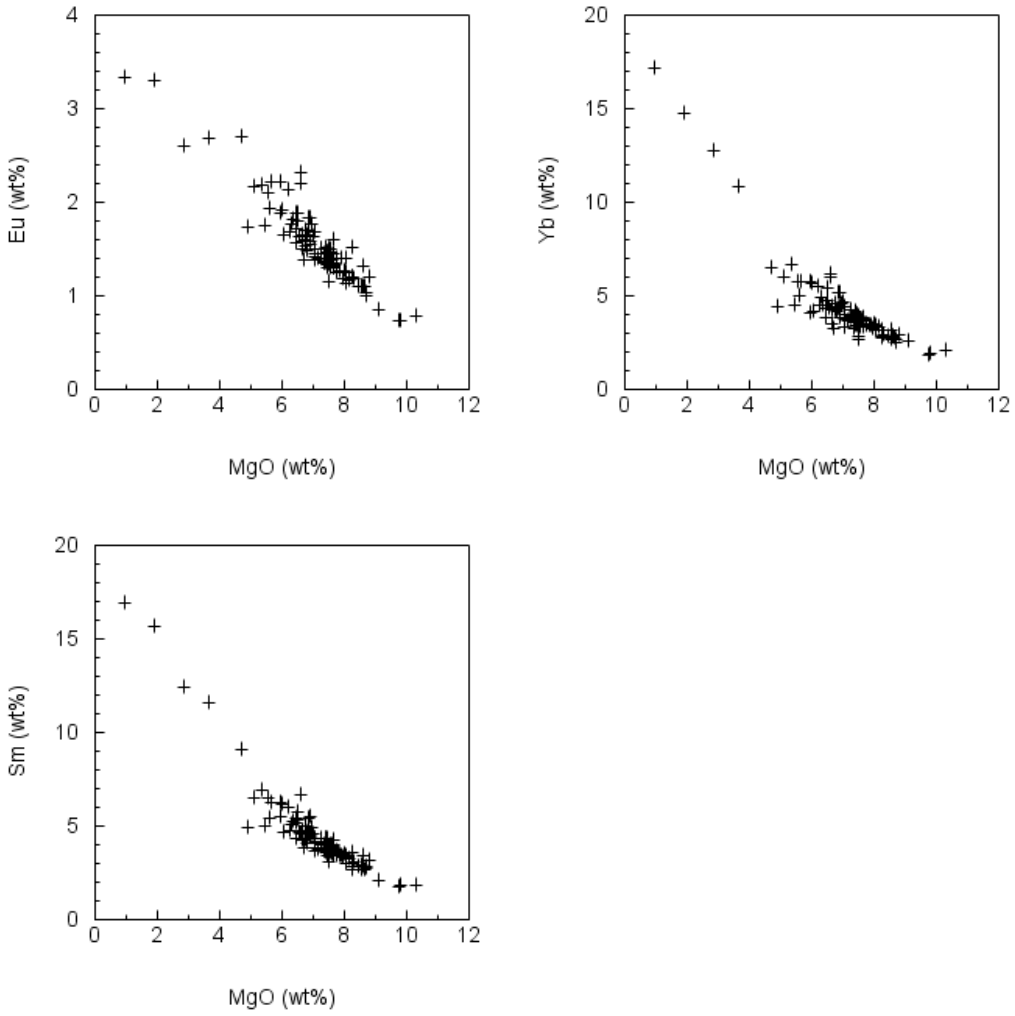

Figure 3. Trace elements Eu, Yb, and Sm plotted against Mg. Data from Gale et al., 2013.

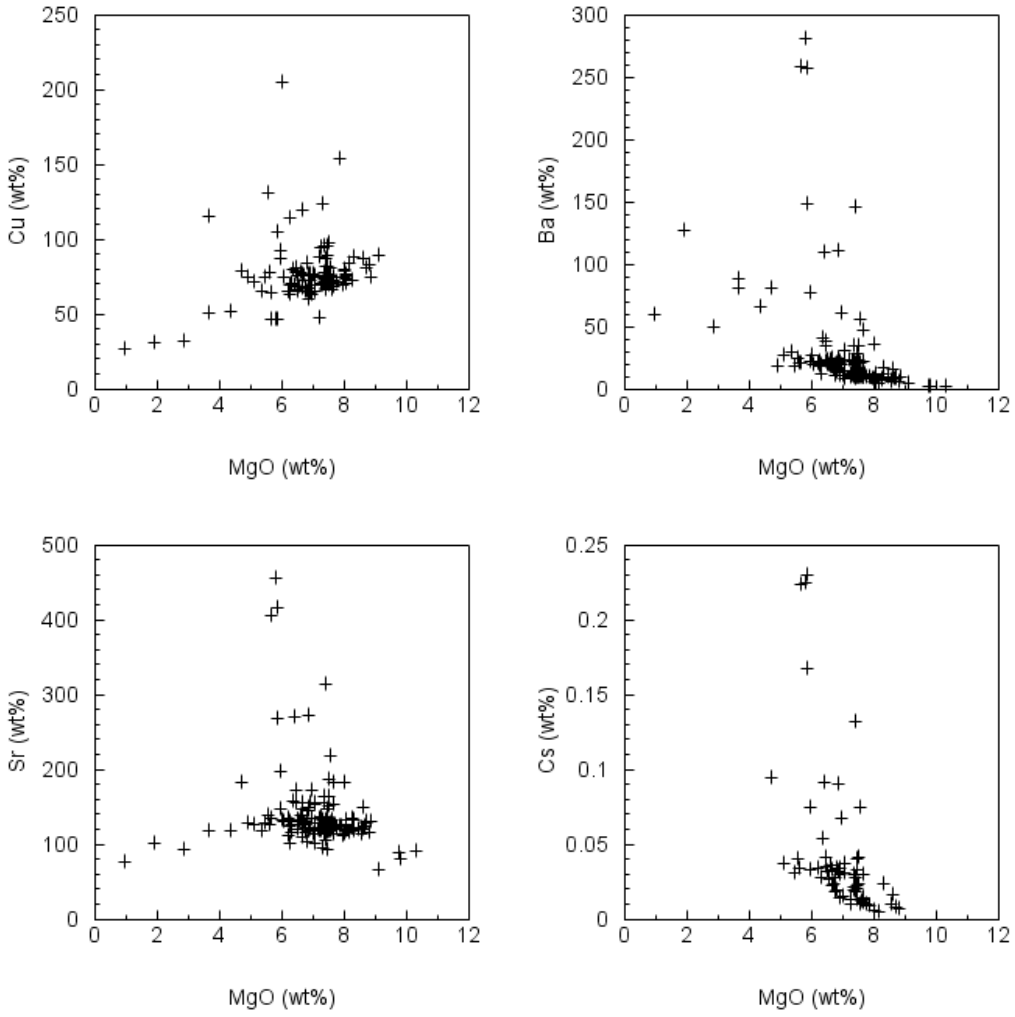

Figure 4. Trace elements Cu, Ba, Sr, and Cs against MgO. Data from Gale et al., 2013.

Rubidium (Rb) and the rare-earth elements (REE) lanthanum (La), and lutetium (Lu) were also plotted against MgO. Lu shows a clear, linearly increasing trend as MgO decreases while Rb and La seem to increase as MgO decreases until about 5 wt% MgO, where both concentrations of Rb and La dramatically increase. (Figure 5).

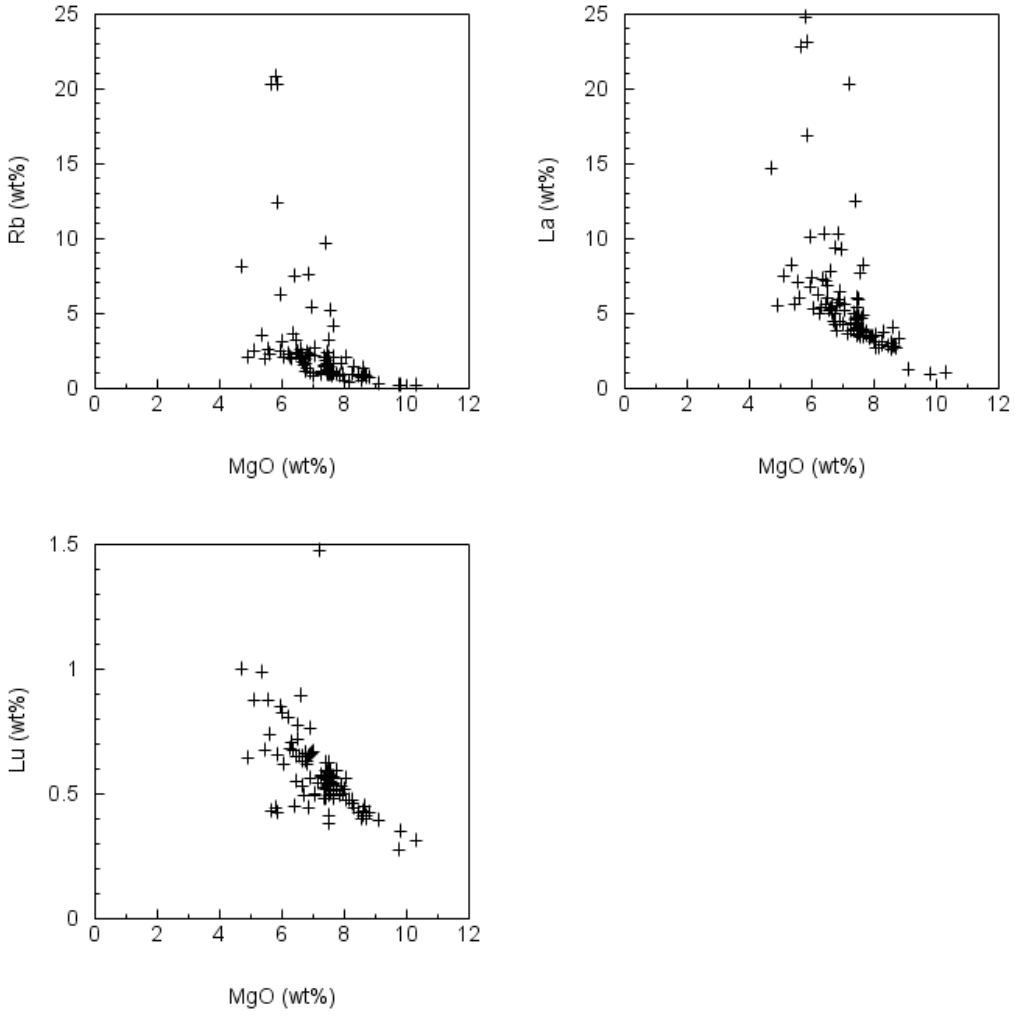

Figure 5. Rare Earth elements Rb, La, and Lu against MgO. Data from Gale et al., 2013.

The elements neodymium (Nd) and zirconium (Zr) are increasing linerarly as MgO decreases (Figure 6).

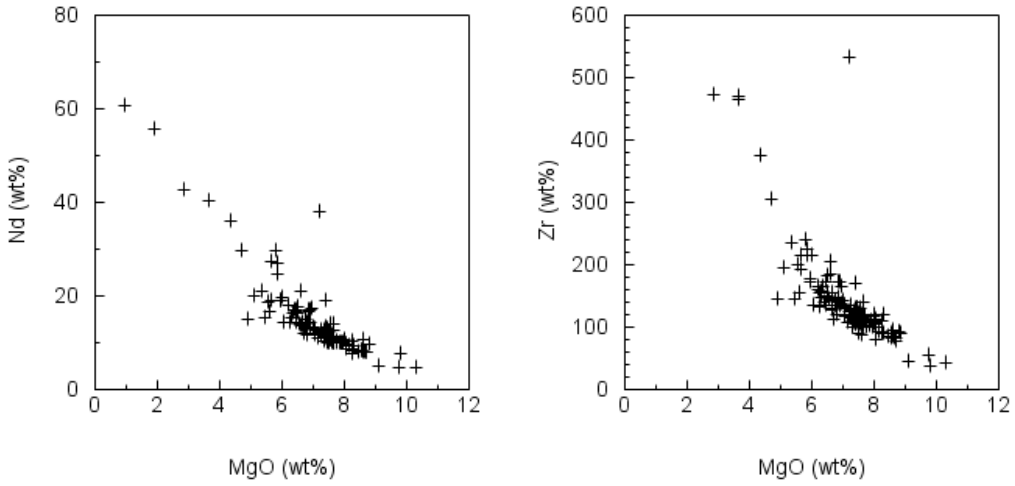

Figure 6. Elements Nd and Zr against MgO. Data from Gale et al., 2013.

Silicon dioxide (SiO_2), titanium oxide (TiO_2), iron oxide (FeO_T), aluminum oxide (Al_2O_3), calcium oxide (CaO), sodium oxide (Na_2O), potassium oxide (K_2O), phosphorous oxide (P_2O_5), and manganese oxide (MnO) are plotted against MgO (Figure 7) to explore relationships in the crystallization of olivine, plagioclase, clinopyroxene, and Fe-Ti oxide. Na_2O, K_2O, and P_2O_5 all increase linearly as MgO decreases. Al_2O_3 and CaO decrease with MgO. SiO_2 decreases up to ~4 wt% MgO and then remains relatively constant at higher values of MgO whereas TiO_2, FeO_T, and MnO increase up to ~4 wt% MgO and decrease at higher values of MgO.

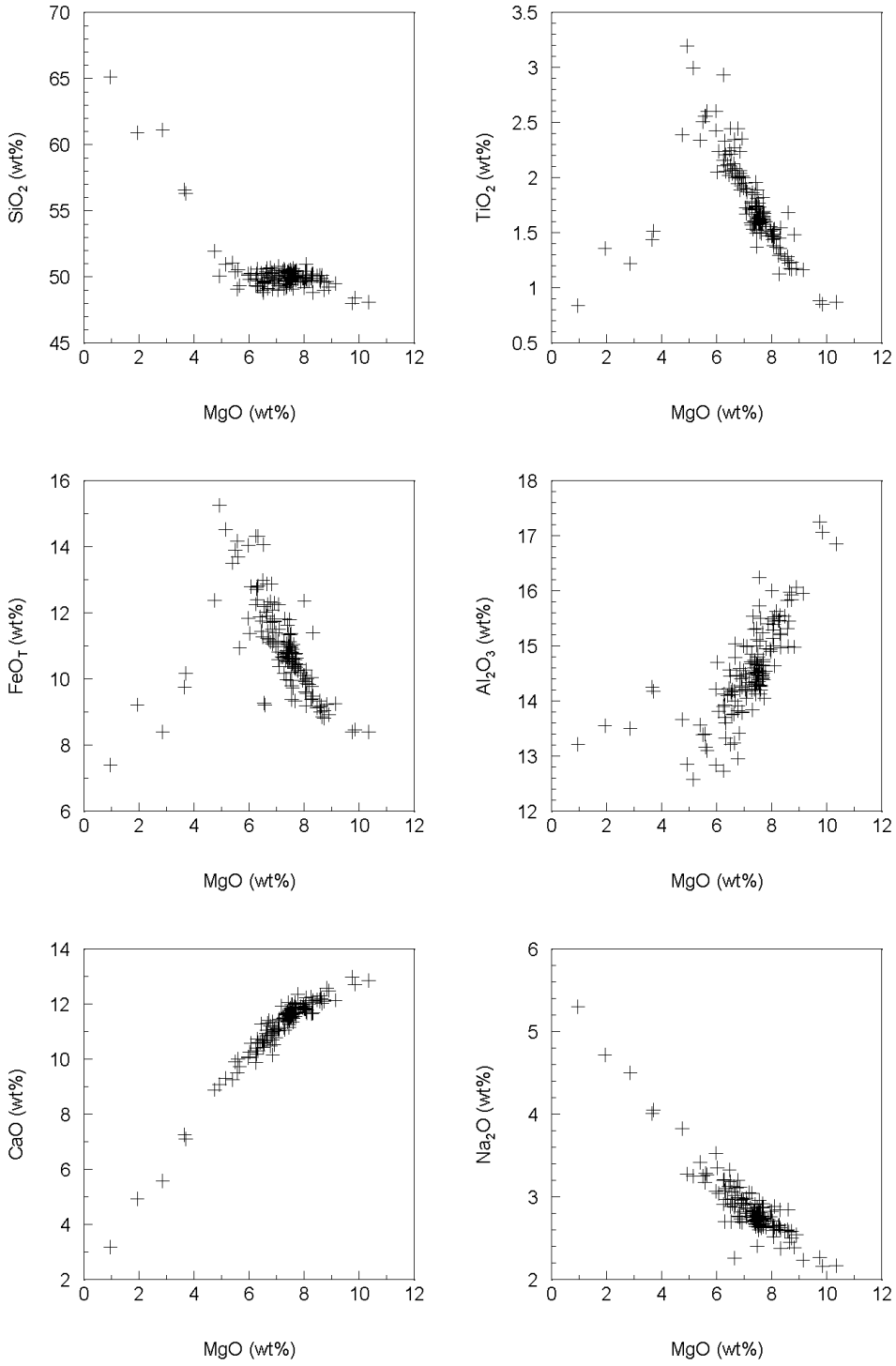

Figure 7a. Oxides plotted against MgO. Data from Gale et al., 2013

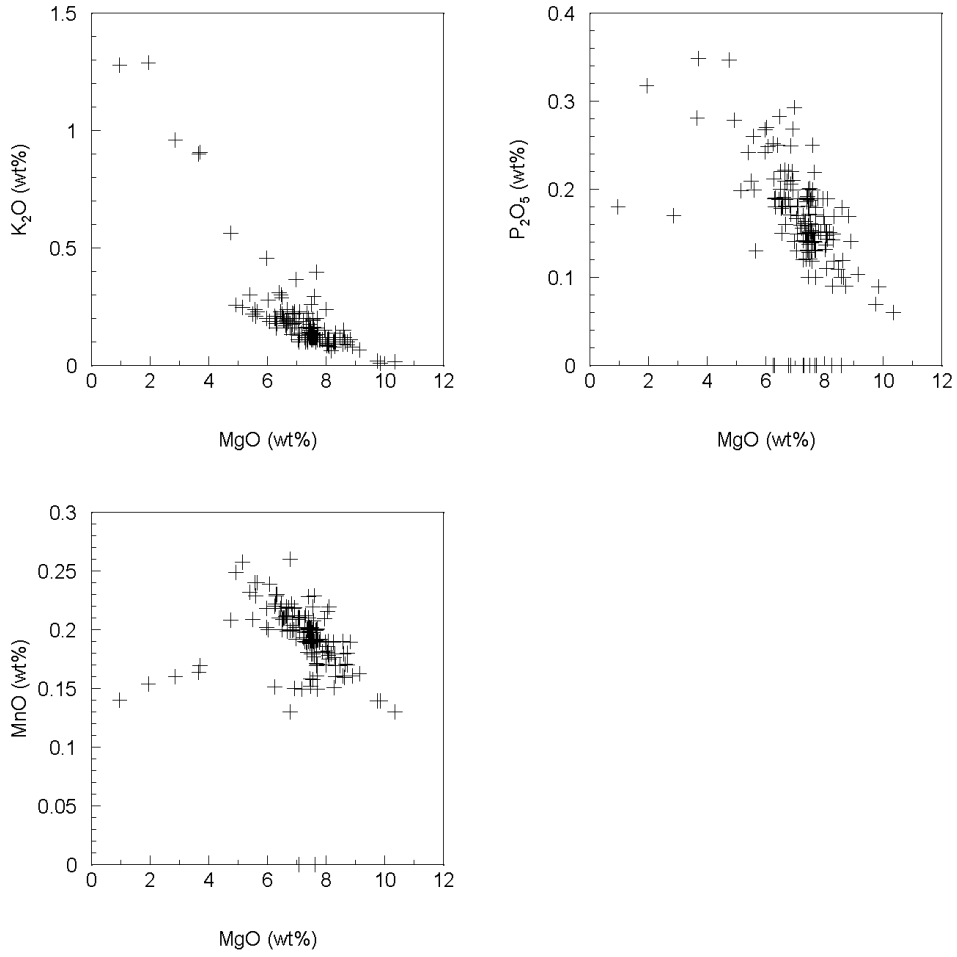

Figure 7b. Oxides plotted against MgO. Data from Gale et al. (2013).

Geochemical Analyses: Trace elements versus trace elements

Plots of trace elements against other trace elements provide a way to observe relationships that indicate how the magma is evolving through cooling and crystallization. Figure 8 shows plots of trace elements La v. Ba, Nb v. Ba, Sm v. La, and Hf v Zr. While the plots of Sm v. La and Hf v. Zr are linear, the plots of La v. Ba and Nb v. Ba show curvature towards Ba at about 30 ppm Ba.

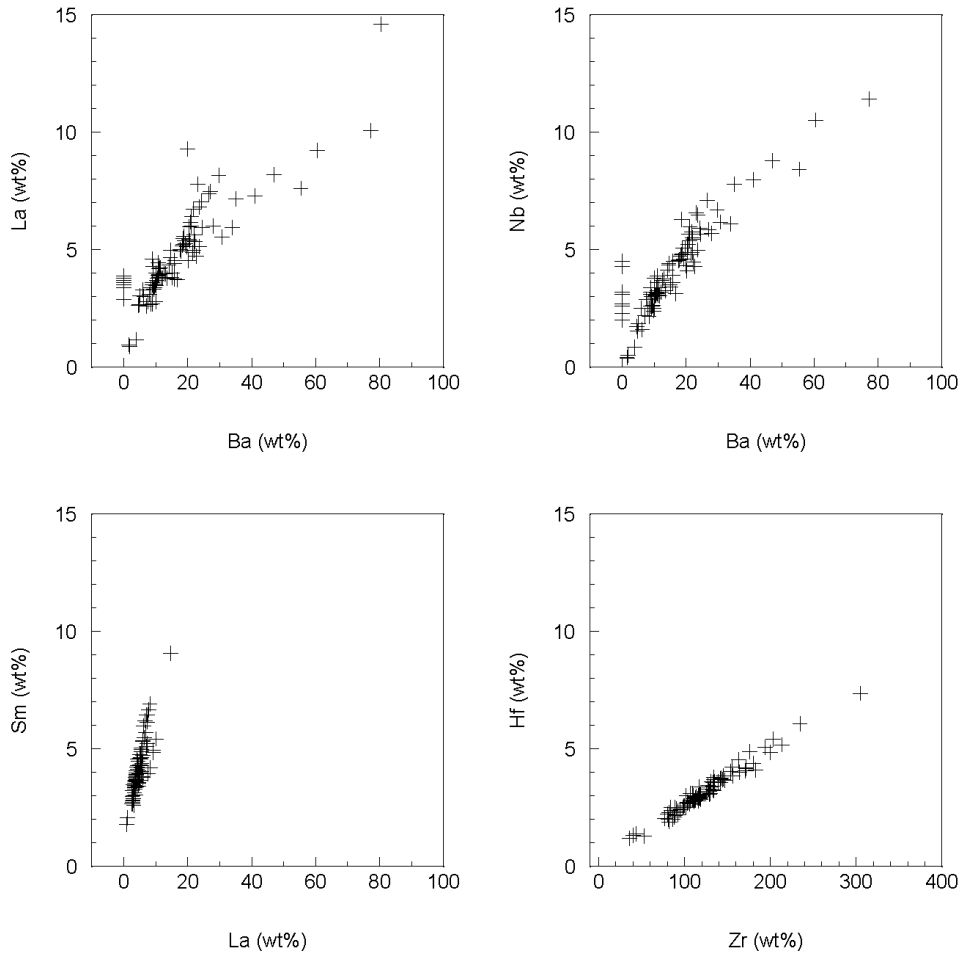

Figure 8. Trace elements plotted against other trace elements. Date from Gale et al., 2013

Geochemical Analyses: Normalized plots

Trace elements normalized to Normal Mid-Ocean Ridge Basalts (NMORB) as defined by Gale et al. (2013) show that most samples have elemental compositions that are enriched relative to NMORB (Figure 9). The dashed line across the graphs is at one, the value at which the magmas would be considered "normal". Concentrations above this line are considered enriched while concentrations below this line are considered depleted. Samples collected from 8.370°N–9.050°N and 11.165°N–11.787°N are more enriched in the incompatible trace elements than are samples from 5.642°N–6.802° and 9.105°N–11.092°N. Negative Sr anomalies for some samples in each of these segments coud be an indication of Sr removal from the melt by crystallization of plagioclase.

REE were normalized to CI chondrite compositions as defined by McDonough and Sun (1995). Some compositions are very enriched in light rare-earths (LREE) compared to the reference value, whereas others show relative depletion in the LREE relative to the HREE (Figure 10). The normalization to primitive mantle as defined by Sun and McDonough (1989) indicates that most samples are also enriched in highly incompatible elements compared to the reference values (Figure 11).

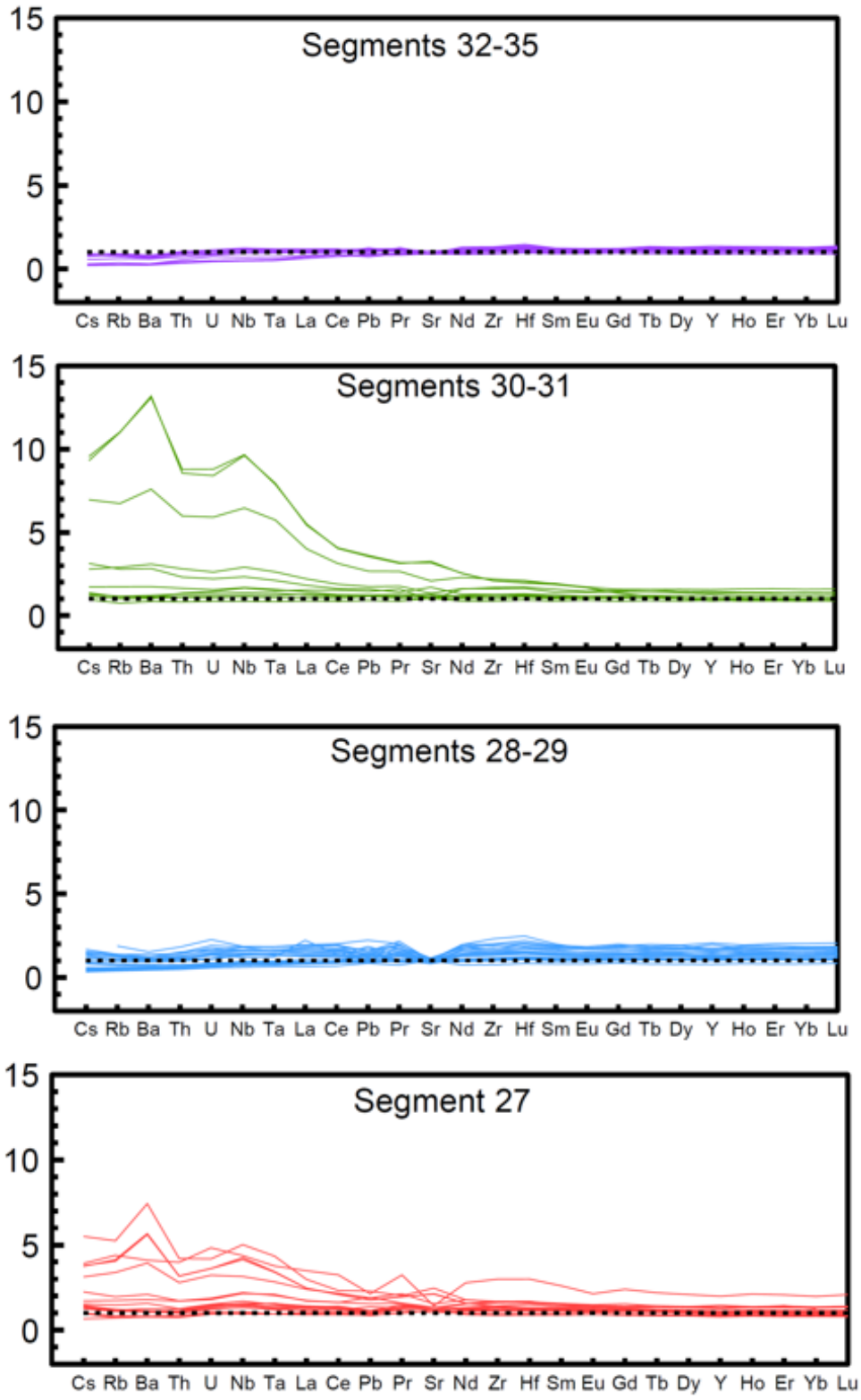

Figure 9. Trace element comositionss normalized to NMORB as defined by Gale et al. (2013). The elements are arranged along the x-axis from most to least incompatible. Because of this arrangement, the plots show how a magma evolves through crystallization.

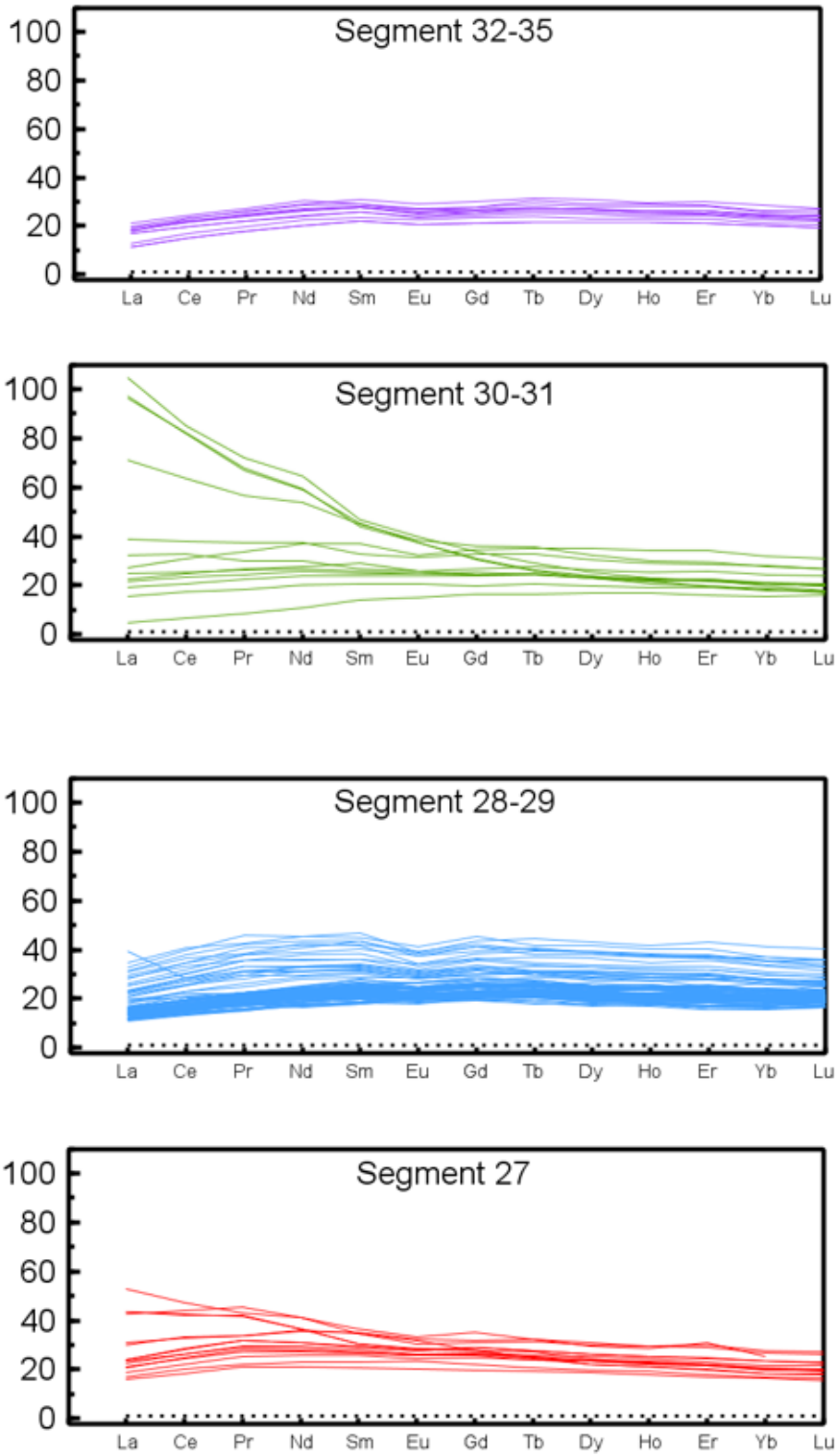

Figure 10. Rare earth elements normalized to chondrites as defined by McDonough and Sun (1995). The elements are arranged from low to high atomic number (atomic weight), but each element is in the same valence state. Because elements with a higher atomic weight create stronger bonds than elements with a low atomic weight, these plots show how a magma evolves by crystallization. Parallel lines show magmas consistent with partial crystallization processes. Curved lines' slopes tell whether the mantle source is enriched or depleted in trace elements.

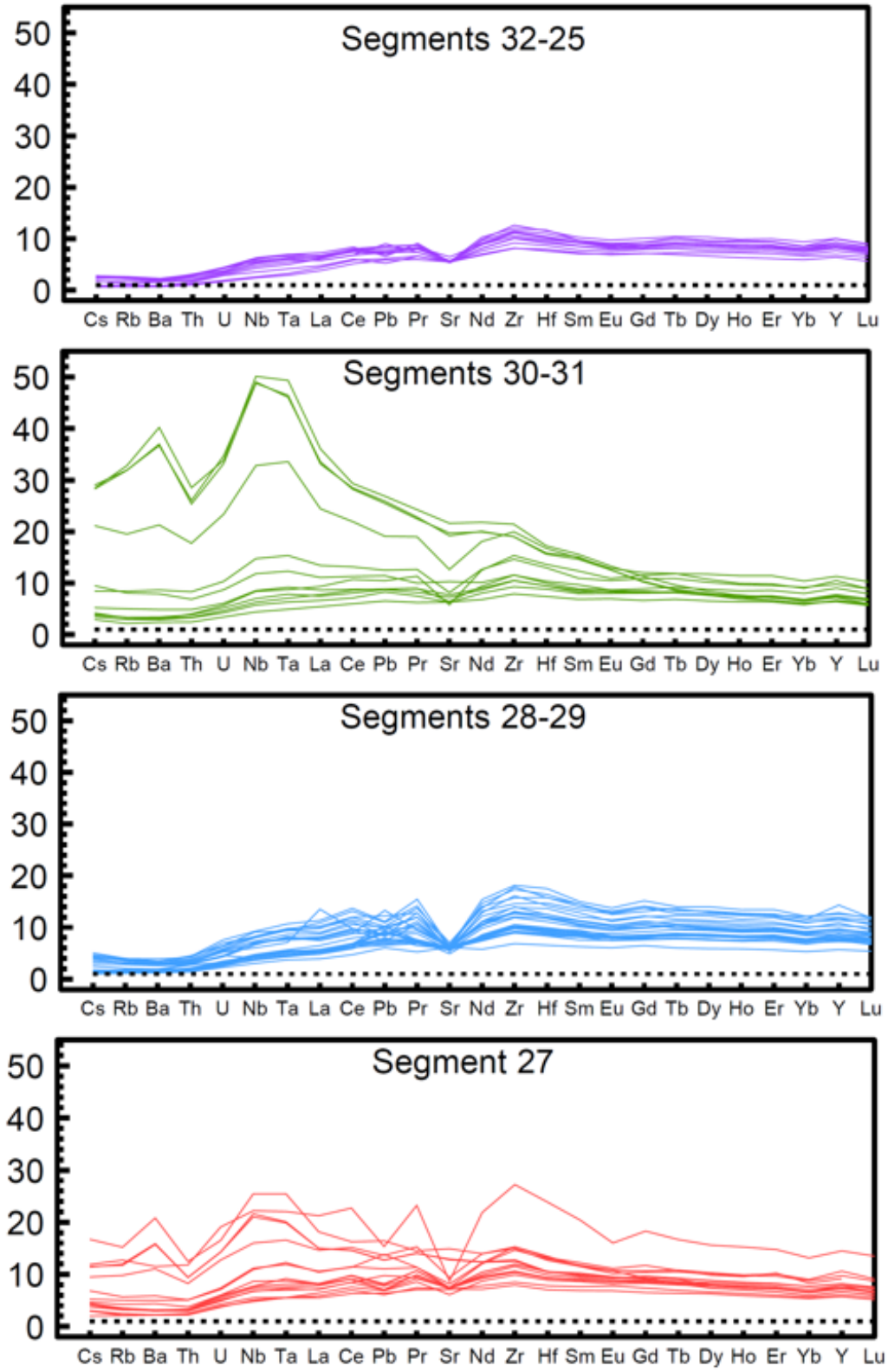

Figure 11. Trace elements normalized to primitive mantle as defined by Sun and McDonough, (1989). Trace elements are organized to show the evolution of magmas from left to right.

Geochemical Analysis: Oxides and ratios versus latitude

Plots of MgO, SiO_2, K_2O/P_2O_5, and K/U versus latitude show how oxides and ratios vary along latitude and relative to transforms and overlapping spreading centers (Figure 12). The two transform faults in this area are the Siqueiros at 8.367°N and the Clipperton at 10.667°N and are indicated on the plots with vertical, green lines. The five overlapping spreading centers in this area are located at 5.50°N, 5.78°N, 9.05°N, 9.88°N, and 11.75°N and are indicated by the vertical, red lines.

Some samples with a large variation in composition are evident on the plots of MgO, SiO_2, and K_2O/P_2O_5 v. latitude. There is an apparent correlation between low MgO, high SiO_2, and high K_2O/P_2O_5 values between the Siqueiros transform and third overlapping spreading center and also just north of the third overlapping spreading center. The concentration of SiO_2 and the K_2O/P_2O_5 and K/U ratios have relatively narrow ranges of concentration along this region of the EPR. The concentration of MgO stays relatively constant except for a decrease in ~2 wt% at the Clipperton transform.

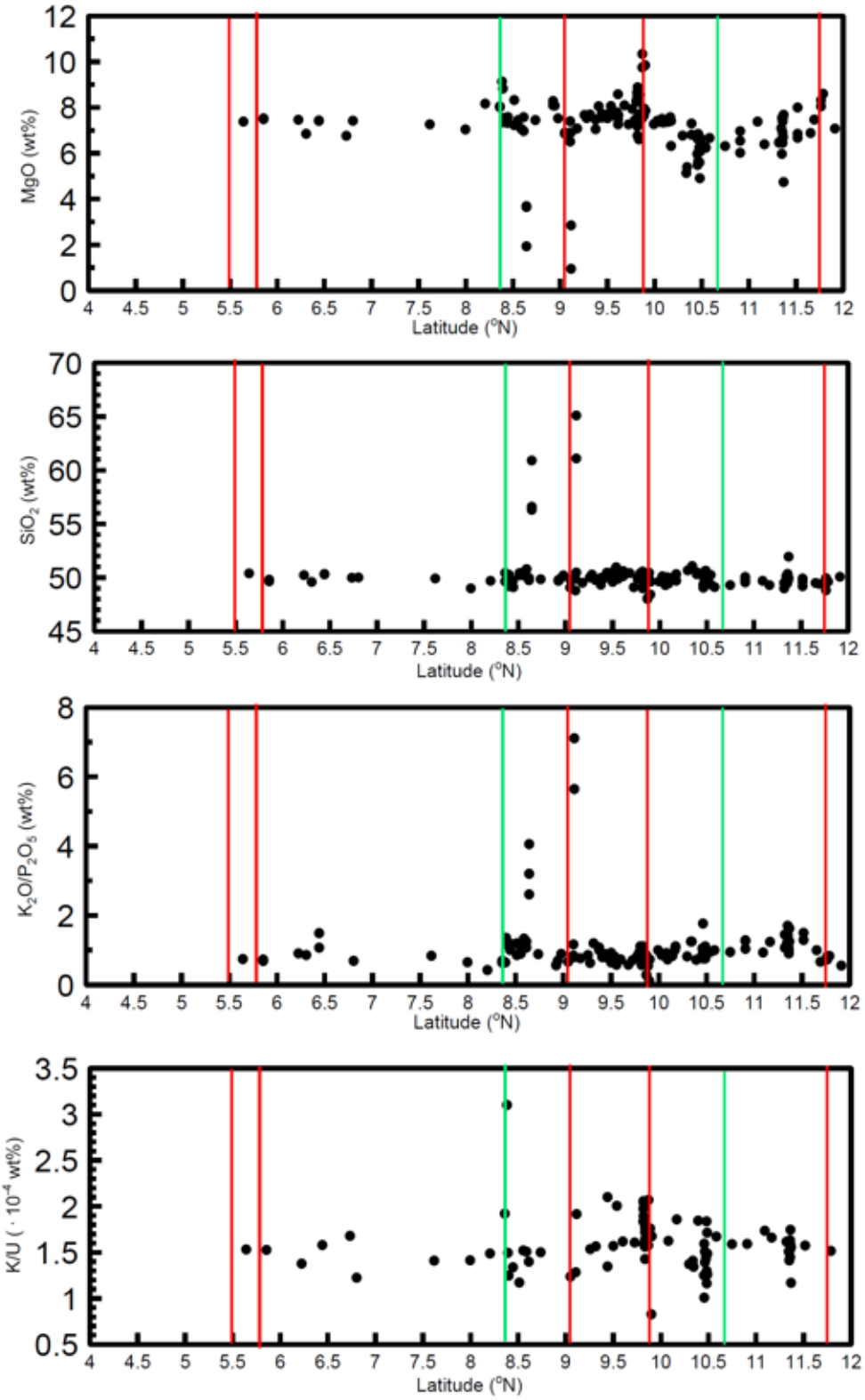

Figure 12. MgO, SiO_2, K_2O/P_2O_5, and K/U plotted against latitude. Red vertical lines indicate overlapping spreading centers and green, vertical lines indicate transforms. The Clipperton transform in located at 10.667°N and the Siqueiros at 8.367°N. Locations of OSCs and transforms from Langmuir (1986). Data from Gale et al. (2013).

Discussion

Trace elements show a large range of concentrations compared to major elements and a study of their abundances in MORB samples is useful for gleaning information on (1) the composition of magmas and rocks in the mantle and (2) how magmas evolve through crystallization.

The variation diagrams shown in Figures 4-7 indicate behavior broadly consistent with magma evolution via crystallization (i.e. incompatible elements increasing with decreasing MgO, compatible elements such as Cu decreasing with decreasing MgO). However, the scatter on plots such as Ba, La, and Sr versus MgO indicates that not all erupted magmas can be derived from a single parent via crystallization.

The plots of CaO and Al_2O_3 versus MgO are consistent with crystallization of olivine, plagioclase and pyroxene during magma evolution. The behavior of TiO_2 and FeO_T are consistent with the onset of crystallization of Fe-Ti oxides as MgO concentrations fall below ~4wt%.

The concentrations of highly incompatible trace elements should, theoretically, increase in residual melts at the same rate. This would produce linear trends on plots of incompatible trace elements versus other incompatible trace elements. Plots of Sm v. La and Hf v. Zr define linear relationships that are consistent with crystallization. However, plots of La v. Ba and Nb v. Ba exhibit non-linear relationships that show enrichment of Ba relative to both La and Nb (Figure 8). This enrichment of Ba cannot be explained by crystallization alone and therefore indicates that there are other processes affecting the chemistry of the magmas such as crustal interaction.

The NMORB defined by Gale et al. (2013) was calculated using a lognormal mean of samples located more than 500 km from plumes. The primitive mantle composition calculated by Sun and McDonough (1989) was calculated by taking an arithmetic mean of samples divided by

chemistry rather than distance-from-plume criteria. Trace elements normalized to NMORB (Figure 9) show that the northern segment of the ridge area (<8.370°N latitude, segments 32-35) is composed of fairly uniform magmas derived from a depleted mantle source. The southern segment of the area contains a wide range of normalized values which could indicate mantle heterogeneity and/or crustal assimilation. Magmas that have trace element compositions that are normal (=1) or enriched (>1) may provide evidence for magma-crust interaction. Magmas that have trace element compositions that are depleted (<1) show evidence for a depleted mantle source region (it is virtually impossible to produce such depletions by interaction with the crust).

The data plotted in Figure 13 can be used to help interpret normalized spider diagrams. The conventional interpretation is that enriched mid-ocean ridge basalts (EMORB) are derived from a mantle source that is enriched in highly incompatible elements relative to NMORB, whereas depleted mid-ocean ridge basalts (DMORB) are derived from a mantle source that is depleted in highly incompatible elements relative to NMORB. Magmas are defined as EMORB if the La/Sm ratio is greater than 1.5 and as DMORB if the ratio is less than 0.8 (Gale et al., 2013). Enrichment is generally attributed to the addition of a "plume-like" component to an NMORB source, whereas depletion is attributed to a previous melt extraction event. However, it is possible that all of these magmas are derived from a depleted source and that EMORB, and possibly also NMORB, compositions are produced by crustal assimilation. However, this inference is speculative and requires additional study.

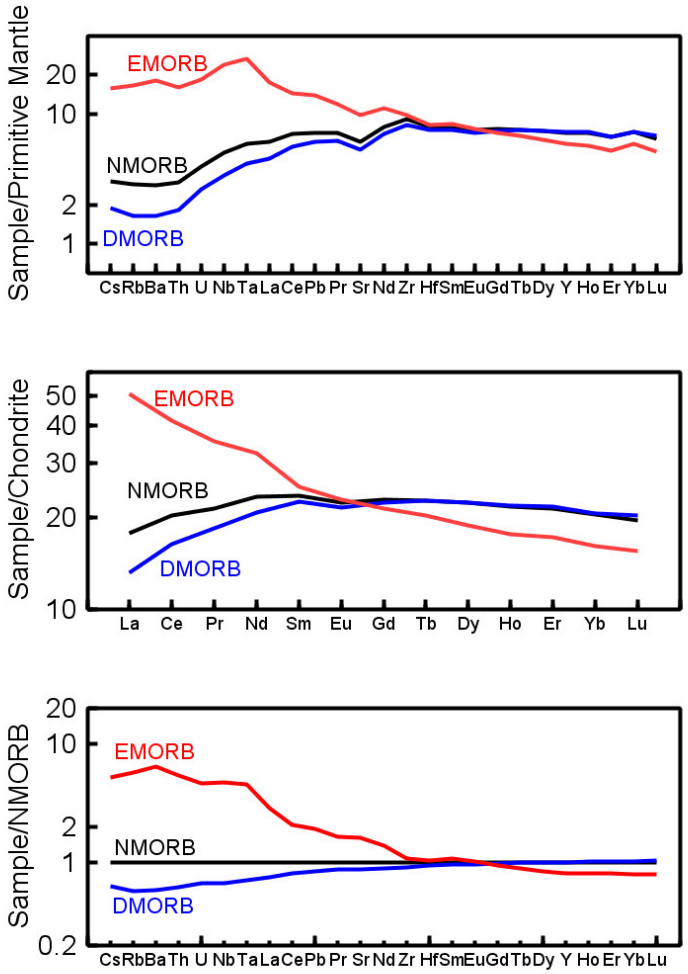

Figure 13. Comparison between EMORB, DMORB, and NMORB using normalization standards for primitive mantle, chondrite, and "normal" mid-ocean basalts. Average compositions defined by Gale et al., 2013.

The plots shown in Figure 11 can be used to interpret magma differentiation, crystallization, and assimilation. Locations with high K_2O, high SiO_2, and low MgO concentrations can be explained by magma differentiation. The correlation between K_2O/P_2O_5 and SiO_2 indicates that either apatite crystallized from evolved magmas—which is unlikely with oceanic basalts because these have P_2O_5 concentrations too low to cause saturation in apatite (Wanless, 2010)—or that assimilation of crustal material is occurring along with crystallization. Because the K/U ratio and SiO_2 do not correlate with one another, there is some uncertainty in the usefulness of K/U ratios for constraining crystallization processes.

Conclusions

With trace element geochemistry, relationships can be observed to describe processes affecting the composition of magmas in this section of the EPR. These include:

(1) Incompatible elements plotted against one another will have a linear relationship if just affected by crystallization. Non-linear relationships show enrichment of one element relative to the other which could provide evidence for the crystallization of specific minerals or, more likely, for crustal assimilation.

(2) Normalized plots show enrichments of trace elements in magmas from 6–12° along the EPR. This could indicate variations in the composition of the mantle source region, or crust-magma interaction.

(3) Correlations between SiO_2, MgO, K_2O/P_2O_5, and K/U can be used to interpret magma differentiation, crystallization, and assimilation. It is important to note when anomalous compositions of a major oxide or trace element coincide with a transform fault or OSC because these features affect the composition of the magmas.

Recommendations for Future Work

In order to continue the study of magma evolution along the Northern EPR, it is important to look at more plots to observe trace element behavior, examine thin section samples, and calculate the pressures of partial crystallization for the magmas in this region of the EPR. Additional analyses done with a Scanning Electron Microscope (SEM) or election probe microanalysis technology would allow measurements of the chemistry of the samples. Isotope ratios plotted against MgO and other isotope ratios can also be used to provide evidence for crustal assimilation.

Current results show evidence for processes other than just crystallization affecting the magmas. We hypothesize that crustal interaction is causing these anomalous compositions but in order to constrain what reactions are taking place to alter the MORB samples, more plots must be created and observed. This way, we can see what trace elements are being enriched or depleted relative to other trace elements and form a better understanding of the processes involved in magma evolution.

Isotope ratios such as $^{87}Sr/^{86}Sr$, $^{143}Nd/^{144}Nd$, $^{206}Pb/^{204}Pb$ (Figure A14) and oxygen isotopes could provide evidence for crustal assimilation or for variations in mantle source compositions (see Wanless et al. 2010, 2012). Isotope ratios can be plotted against MgO to observe relationships during crystallization or against other ratios. While isotope ratio plots were created, this thesis does not interpret them and could be a point of interest in future work.

Thin section analyses allow for identification of the minerals crystallized from the basalt samples. Minerals that show zoning would suggest abrupt changes in temperature, pressure, or melt composition. Minerals with corroded edges suggest resorption and minerals with resorbed cores suggest mixing of the melt. Samples with glass matrices suggest devitrification.

Calculation of the pressures for partial crystallization would provide insight on the "pressure paradox" (Zerda, 2014) of anomalously high pressures calculated for samples from the EPR. Zerda's results conflict with Herzberg's (2004) contention that high pressures are often associated with transforms. High pressures calculated by Zerda for the EPR between 11°N and 13°N do not appear to correlate with transforms. Calculated pressures from this region of the EPR would provide evidence to either support or refute the possibility that high pressures along the EPR are artifacts of anomalous chemistry, and are not representative of the actual crystallization regime along the ridge axis.

REFERENCES CITED

Almeev, R., Holtz, F., Koepke, J., Haase, K., and Devey, C., 2008, Depths of partial crystallization of H2O-bearing MORB: Phase equilibria simulations of basalts at the MAR near Ascension Island (7-11 degrees S): Journal of Petrology, v. 49, no. 1, p. 25-45. doi: 10.1093/petrology/egm068

Bown, J.W., and White, R.S., 1994, Variation with spreading rate of oceanic crustal thickness and geochemistry: Earth and Planetary Science Letters, v. 121, no. 3-4, p. 435-449. doi: 10.1016/0012-821X(94)90082-5

DeMets, C., Gordon, R.G., and Argus, D.F., 2010, Geologically current plate motions: Geophysical Journal International, v. 181, no. 1, p. 1-80. doi: 10.1111/j.1365-246X.1990.tb06579.x

Demets, C., Gordon, R.G., Argus, D.F., and Stein, S., 1990, Current plate motions: Geophysical Journal International, v. 101, no. 2, p. 425-478. doi:10.1111/j.1365-246X.2009.04491.x

Dmitriev, L.V., 1998, Chemical variability of mid-ocean ridge basalts as a function of the geodynamic setting of their formation: Petrology, v. 6, no. 4, p. 314-334.

Francheteau, J., 1983, The oceanic-crust: Scientific American, v. 249, no. 3, p. 114-129. doi:10.1038/scientificamerican0983-114

Gale, A., Dalton, C.A., Langmuir, C.H., Su, Y., and Schilling, J.G., 2013, The mean composition of ocean ridge basalts: Geochemistry Geophysics Geosystems, v. 14, no. 3, p. 489-518. doi: 10.1029/2012GC004334

Henstock, T.J., Woods, A.W., and White, R.S., 1993, The accretion of oceanic-crust by episodic sill intrusion: Journal of Geophysical Research-Solid Earth, v. 98, no. B3, p. 4143-4161. doi: 10.1029/92JB02661

Herzberg, C., 2004, Partial crystallization of mid-ocean ridge basalts in the crust and mantle: Journal of Petrology, v. 45, no. 12, p. 2389-2405. doi: 10.1093/petrology/egh040

Kelemen, P.B., Hirth, G., Shimizu, N., Spiegelman, M., and Dick, H.J.B., 1997, A review of melt migration processes in the adiabatically upwelling mantle beneath oceanic spreading ridges: Philosophical Transactions of the Royal Society a-Mathematical Physical and Engineering Sciences, v. 355, no. 1723, p. 283-318. doi: 10.1098/rsta.1997.0010

Keller, R.A., Fisk, M.R., White, W.M., and Birkenmajer, K., 1992, Isotopic and trace-element constraints on mixing and melting models of marginal basin volcanism, Bransfield Strait, Antarctica: Earth and Planetary Science Letters, v. 111, no. 2-4, p. 287-303. doi: 10.1016/0012-821X(92)90185-X

Kelley, D.F., and Barton, M., 2008, Pressures of crystallization of Icelandic magmas: Journal of Petrology, v. 49, no. 3, p. 465-492. doi: 10.1093/petrology/egm089

Korenaga, J., and Kelemen, P. B., 1998, Melt migration through the oceanic lower crust: a constraint from melt percolation modeling with finite solid diffusion: Earth and Planetary Science Letters, v. 156, no. 1-2, p. 1-11. doi: 10.1016/S0012-821X(98)00004-1

Langmuir, C.H., Bender, J.F., and Batiza, R., 1986, Petrological and tectonic segmentation of the East Pacific Rise, 5-degrees-30'-14-degrees-30'-N: Nature, v. 322, no. 6078, p. 422-429. doi: 10.1038/322422a0

Lissenberg, J., and Dick, H.J.B., 2008, Melt-rock reaction in the lower oceanic crust and its implications for the genesis of mid-ocean ridge basalt: Earth and Planetary Science Letters, v. 271, no. 1-4, p. 311-325. doi: 10.1016/j.epsl.2008.04.023

Macdonald, K.C., and Fox, P.J., 1990, The mid-ocean ridge: Scientific American, v. 262, no. 6, p. 72-79.

Macdonald, K.C., 2001, Mid-ocean ridge tectonics, volcanism and geomorphology, *in* Steele, J., ed., Encyclopedia of Ocean Sciences, 1st edition: Academic Press, 1798-1813.

Maclennan, J., Hulme, T., and Singh, S.C., 2004, Thermal models of oceanic crustal accretion: Linking geophysical, geological and petrological observations: Geochemistry Geophysics Geosystems, v. 5. doi: 10.1029/2003GC000605

McDonough, W.F., and Sun, S.S., 1995, The composition of the Earth: Chemical Geology, v. 120, no. 3-4, p. 223-253. doi: 10.1016/0009-2541(94)00140-4

Michael, P.J., and Cornell, W.C., 1998, Influence of spreading rate and magma supply on crystallization and assimilation beneath mid-ocean ridges: Evidence from chlorine and major element chemistry of mid-ocean ridge basalts: Journal of Geophysical Research-Solid Earth, v. 103, no. B8, p. 18325-18356. doi: 10.1029/98JB00791

Morgan, J.P., and Chen, Y.J., 1993, Dependence of ridge-axis morphology on magma supply and spreading rate: Nature, v. 364, no. 6439, p. 706-708.

Reynolds, J.R., Langmuir, C.H., Bender, J.F., Kastens, K.A., and Ryan, W.B.F., 1992, Spatial and temporal variability in the geochemistry of basalts from the East Pacific Rise: Nature, v. 359, no. 6395, p. 493-499. doi: 10.1038/ngeo504

Rubin, K.H., and Sinton, J.M., 2007, Inferences on mid-ocean ridge thermal and magmatic structure from MORB compositions: Earth and Planetary Science Letters, v. 260, no. 1-2, p. 257-276. doi: 10.1016/j.epsl.2007.05.035

Rubin, K.H., Sinton, J.M., Maclennan, J., and Hellebrand, E., 2009, Magmatic filtering of mantle compositions at mid-ocean-ridge volcanoes: Nature Geoscience, v. 2, no. 5, p. 321-328.

Sinton, J.M., and Detrick, R.S., 1992, Mid-ocean ridge magma chambers: Journal of Geophysical Research-Solid Earth, v. 97, no. B1, p. 197-216. doi: 10.1029/91JB02508

Sun, S.S., and McDonough, W.F., 1989, Chemical and isotopic systematics of oceanic basalts: Implications for mantle composition and processes: Geological Society, London, v. 42, p. 313-345. doi: 10.1144/GSL.SP.1989.042.01.19

Wanless, V.D., Perfit, M.R., Ridley, W.I., and Klein, E.M., 2010, Dacite petrogenesis on mid-ocean ridges: evidence for oceanic crustal melting and assimilation: Journal of Petrology, v. 51, no. 12, p. 2377-2410. doi: 10.1093/petrology/egq056

Wanless, V.D., Perfit, M.R., Ridley, W.I., Wallace, P.J., Grimes, C.B., and Klein, E.M., 2011, Volatile abundances and oxygen isotopes in basaltic to dacitic lavas on mid-ocean ridges: The role of assimilation at spreading centers: Chemical Geology, v. 287, no. 1-2, p. 54-65. doi: 10.1016/j.chemgeo.2011.05.017

White, W.M., 1997, Geochemistry: Oxford, Wiley-Blackwell, 701 p.

Zerda, C., 2014, Partial crystallization in the deep crust at the East Pacific Ridge: A study from 8° to 14°N [Undergraduate thesis]: The Ohio State University, 36 p.

APPENDIX

Segment	Latitude
26	11.765°N - 11.913°N
27	11.165°N - 11.787°N
28	10.287°N - 11.092°N
29	9.105°N - 10.175°N
30	8.400°N - 9.050°N
31	8.370°N - 8.383°N
32	8.392°N
33	8.204°N - 8.360°N
34	7.618°N - 7.995°N
35	5.642°N - 6.802°N

Table A1. Segments as defined by Gale et al. and their corresponding latitudes

Trace Element	NMORB Concentration
Cs	**0.024**
Rb	**1.84**
Ba	**19.6**
Th	**0.252**
U	**0.083**
Nb	**3.62**
Ta	**0.24**
La	**4.19**
Ce	**12.42**
Pb	**0.51**
Pr	**1.98**
Sr	**128**
Nd	**10.66**
Zr	**101.9**
Hf	**2.46**
Sm	**3.48**
Eu	**1.26**
Gd	**4.55**
Tb	**0.82**
Dy	**5.5**
Y	**33.2**
Ho	**1.18**
Er	**3.42**
Yb	**3.28**
Lu	**0.48**
Cr	**263**
Ni	**100**
Sc	**38.4**
V	**280**

Table A2. NMORB concentrations from Gale et al., 2013

Trace Element	REE Concentation
La	0.237
Ce	0.613
Pr	0.0928
Nd	0.457
Sm	0.148
Eu	0.0563
Gd	0.199
Tb	0.0361
Dy	0.246
Ho	0.0546
Er	0.16
Yb	0.161
Lu	0.0246

Table A3. REE/Chondrite concentrations from McDonough and Sun, 1995

Trace Element	PrimMant Concentation
Cs	0.0079
Rb	0.635
Ba	6.989
Th	0.085
U	0.021
Nb	0.713
Ta	0.041
La	0.687
Ce	1.775
Pb	0.071
Pr	0.276
Sr	21.1
Nd	1.354
Zr	11.2
Hf	0.309
Sm	0.444
Eu	0.168
Gd	0.596
Tb	0.108
Dy	0.737
Ho	0.164
Er	0.48
Yb	0.493
Y	4.55
Lu	0.074

Table A4. Primitive Mantle concentration from Sun and McDonough, 1989

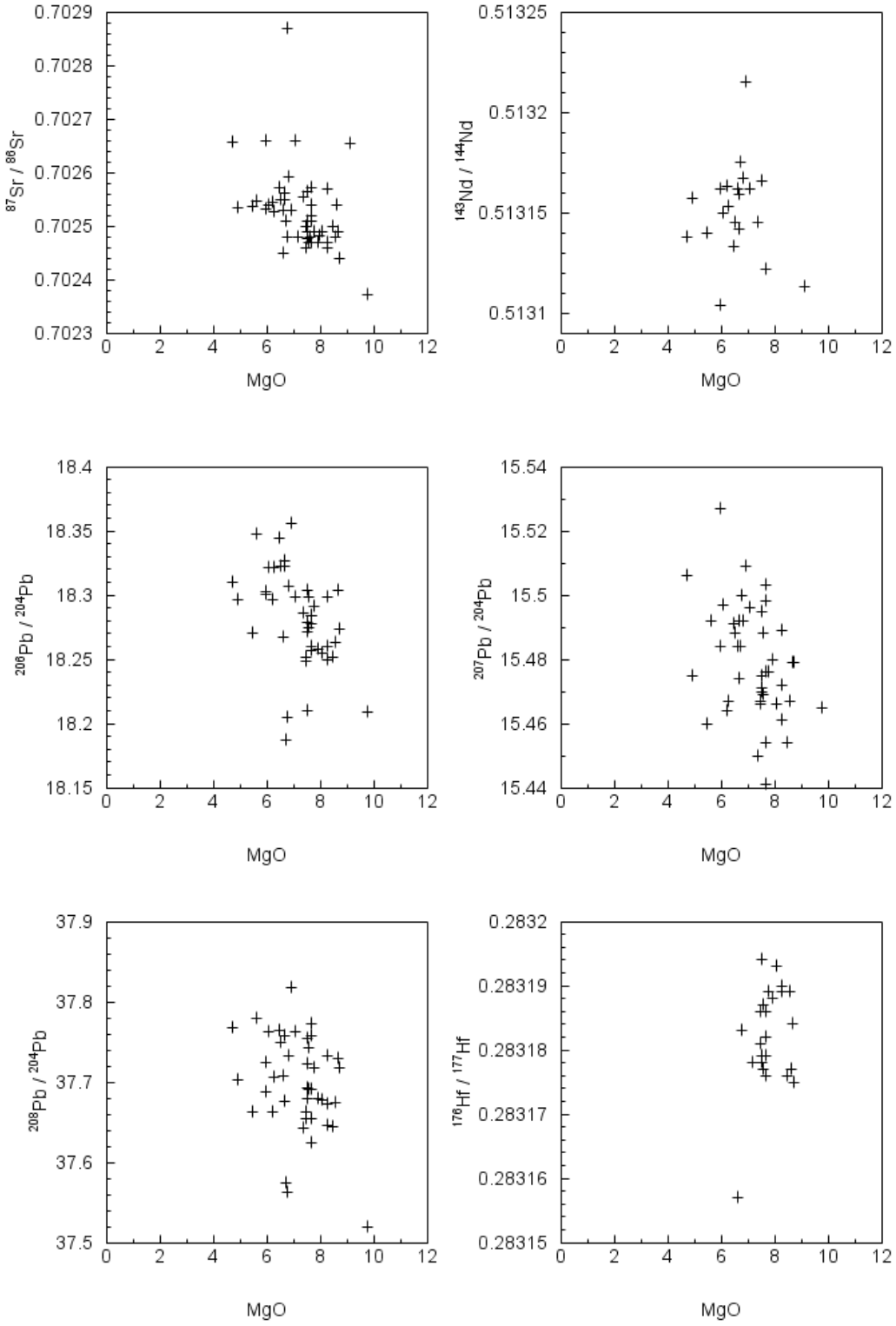

Figure A14. Isotope ratios plotted against MgO. Data from Gale et al., 2013.

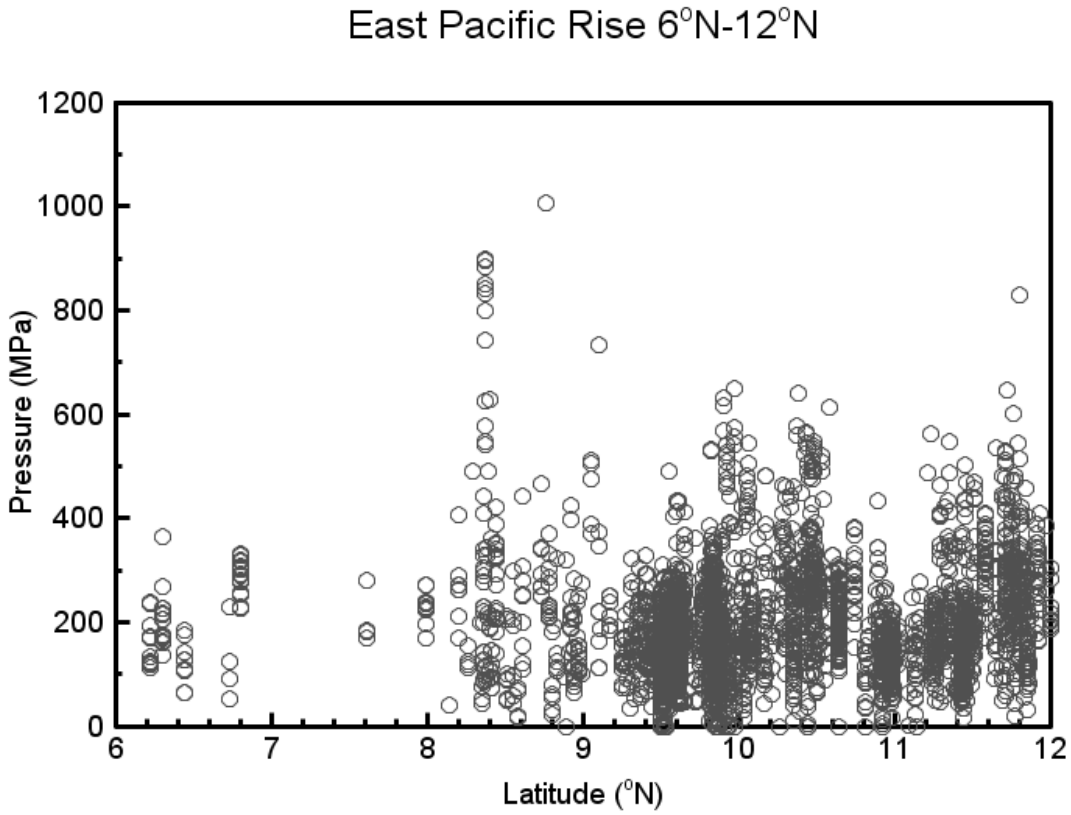

Figure A15. Pressures calculated by Zerda (2014) along latitude for the EPR.

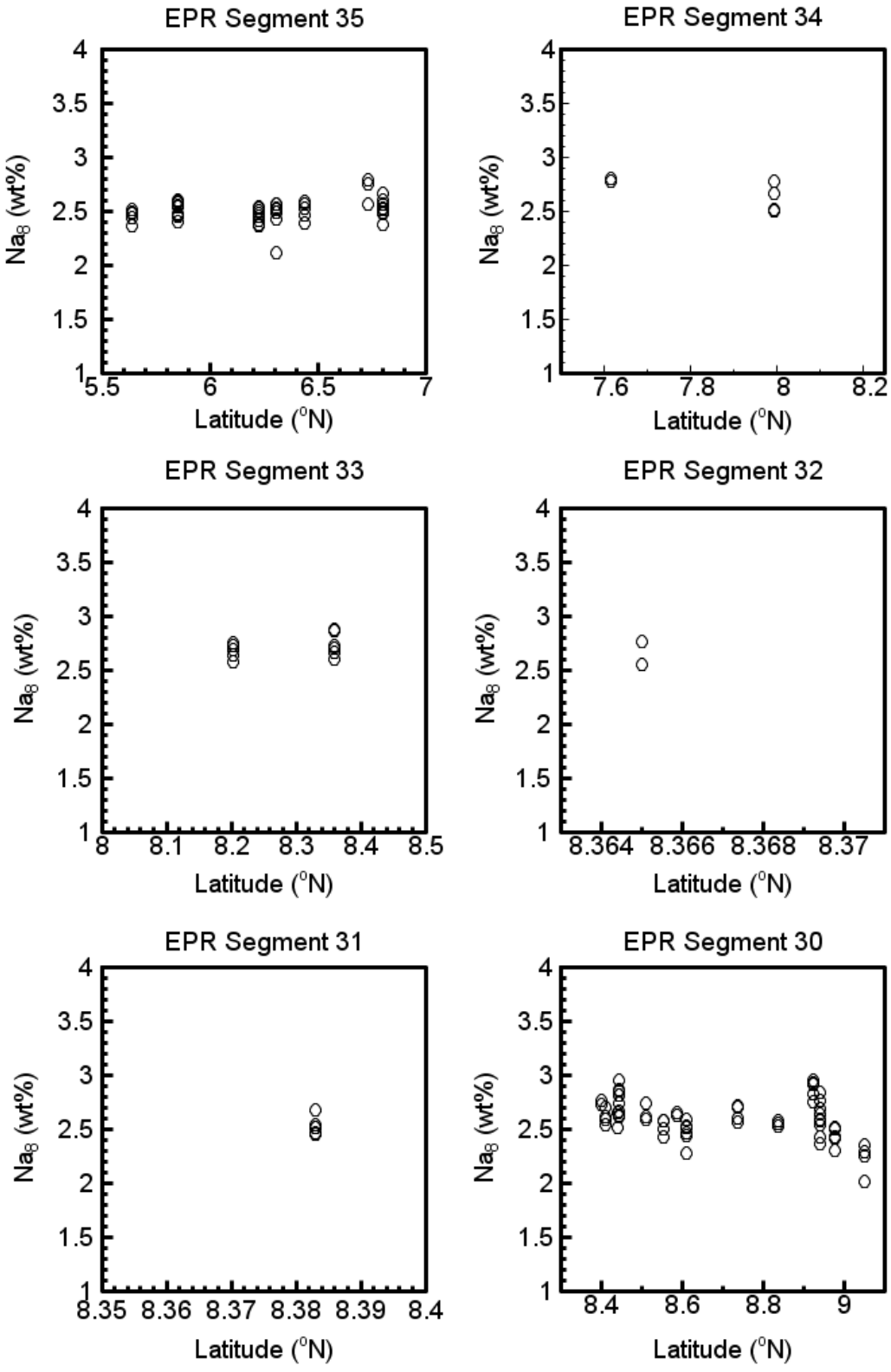

Figure A16a. Na_8 weight percent for EPR Segments 30-35. Calculated by Zerda (2014).

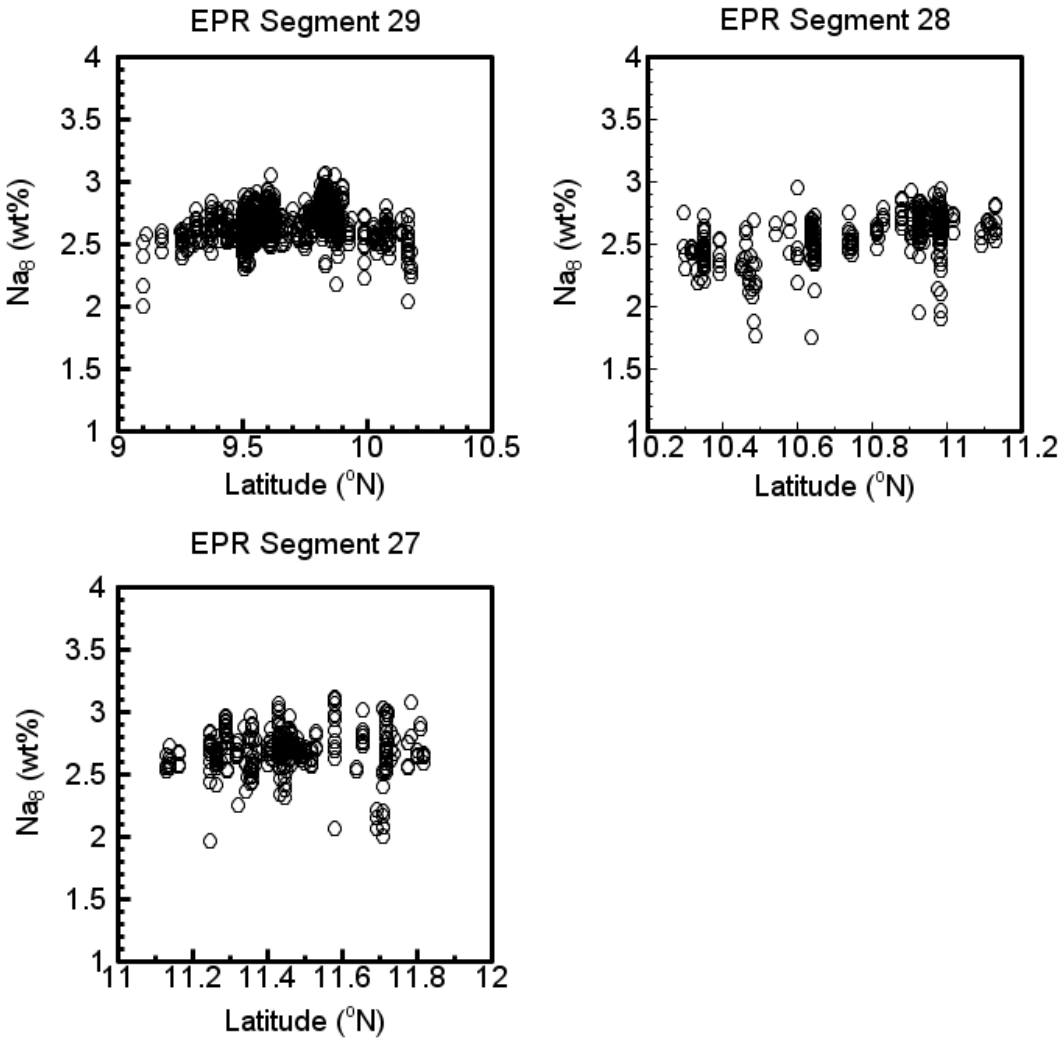

Figure A16b. Na_8 weight percent for EPR Segments 27-29. Calculated by Zerda (2014).